IAC-07-C1.7.03

Optimal Reconfiguration Maneuvers for Spacecraft Imaging Arrays in Multi-Body Regimes

Lindsay D. Millard
Graduate Student
School of Aeronautics and Astronautics
Purdue University
West Lafayette, Indiana
lmillard@purdue.edu

Kathleen C. Howell
Hsu Lo Professor of Aeronautical and Astronautical Engineering
School of Aeronautics and Astronautics
Purdue University
West Lafayette, Indiana
howell@purdue.edu

Abstract

Upcoming National Aeronautics and Space Administration (NASA) mission concepts include satellite arrays to facilitate imaging and identification of distant planets. These mission scenarios are diverse, including designs such as the Terrestrial Planet Finder-Occulter (TPF-O), where a monolithic telescope is aided by a single occulter spacecraft, and the Micro-Arcsecond X-ray Imaging Mission (MAXIM), where as many as sixteen spacecraft move together to form a space interferometer. Each design, however, requires precise reconfiguration and star-tracking in potentially complex dynamic regimes. This paper explores control methods for satellite imaging array reconfiguration in multi-body systems. Specifically, optimal nonlinear control and geometric control methods are derived and compared to the more traditional linear quadratic regulators, as well as to input state feedback linearization. These control strategies are implemented and evaluated for the TPF-O mission concept.

Introduction

Over the next two decades, one focus of NASA's *Origins* program is the development of sophisticated telescopes and technologies to begin a search for extraterrestrial life and to monitor the birth of neighboring galaxies. Part of the program's mission is to (1) locate and image Earth-like planets orbiting other stars; and (2) determine the probability that life has existed or could develop on the surface.[1]

Traditional Earth-based telescopes must continuously expand in size to resolve increasingly distant and faint objects. Unfortunately, as the size of a telescope increases, it becomes too heavy and too expensive to launch, thus motivating alternative designs for deep-space observers. One such example is a free-flying array or constellation of smaller satellites that work together to form a single optical platform.

Upcoming National Aeronautics and Space Administration (NASA) mission concepts include satellite formations to facilitate imaging and identification of distant planets. These scenarios are diverse, including designs such as the Terrestrial Planet Finder-Occulter (TPF-O),[2] where a monolithic telescope is aided by a single occulter spacecraft, and the Micro-Arcsecond X-ray Interferometry Mission (MAXIM),[3] where as many as sixteen spacecraft move together to form a space interferometer. Each design, however, requires precise reconfiguration and star-tracking in potentially complex dynamic regimes. Numerous inter-spacecraft positioning and system geometry constraints must be satisfied to assure successful imaging. Spacecraft separated over large distances must constantly be re-oriented and pointed at different stars, while the distance between the vehicles is expanding and contracting. All must be

accomplished with minimum fuel expenditure, and for many missions, autonomously.

Extensive progress in spacecraft formation control has been achieved. Previously, the focus for much of the analysis was on satellites moving under the gravitational influence of the Earth, or simply in free-space.[4,5] Recently, however, potential also applications involve satellite arrays near the collinear libration points and, consequently, generate considerable interest in formation control strategies in multi-body regimes.[6-14]

Howell and Marchand successfully apply both discrete and continuous control methods to deploy, enforce, and reconfigure formations near the vicinity of libration points in the Sun-Earth/Moon system.[15,16] Specifically, these methods include input-state and input-output feedback linearization, linear quadratic regulator theory, and impulsive maneuvers derived via a differential corrections scheme. In their examples, spacecraft follow both natural and non-natural trajectories in the Circular Restricted 3-Body Problem (CR3PB). This analysis is also transitioned to an ephemeris model, including solar radiation pressure.

Marchand and Howell further indicate that the required discrete velocity changes for individual satellites within a formation are often impossibly small, considering current thruster capabilities.[17] Carlson, Pernicka, and Balakrishnan expand upon this result via the development of a method for identification of formation size and control tolerances for which impulsive maneuvers become a practical option.[18,19] This research focuses on the analysis of discrete maneuvering techniques using differential corrections in the CR3BP.

Very recently, control of interferometric satellite arrays has been pursued. Because of the complexity of the problem, much of the available research assumes satellites within the formation are moving through free space.[20-25] However, Millard and Howell develop two control strategies that are advantageous for interferometric imaging arrays in multi-body regimes. A continuous geometric control algorithm is based on the dynamical characteristics of the phase space near periodic orbits.[26] By adjusting parameters in the control algorithm appropriately, satellites in the formation follow trajectories that aid image reconstruction. Secondly, a nonlinear, locally-optimal control law is developed that minimizes fuel while optimizing image resolution in the CR3BP.[27]

The goal in the present investigation is a comparison of control methods for array re-configuration in multi-body systems. Specifically, optimal nonlinear control as well as geometric control methods are derived and compared to more traditional linear quadratic regulators and feedback linearization. The control strategies are implemented and evaluated for the TPF-O mission concept.

DYNAMIC MODEL: CR3BP

The motion of a spacecraft in the CR3BP is described in terms of rotating coordinates relative to the barycenter of the system primaries. For this analysis, emphasis is placed on formations near the libration points in the Sun-Earth/Moon system. Thus, the rotating *x*-axis is directed from the Sun toward the Earth/Moon barycenter. The *z*-axis is normal to the plane of motion of the primaries, and the *y*-axis completes the right-handed triad. The system is represented in Figure 1.

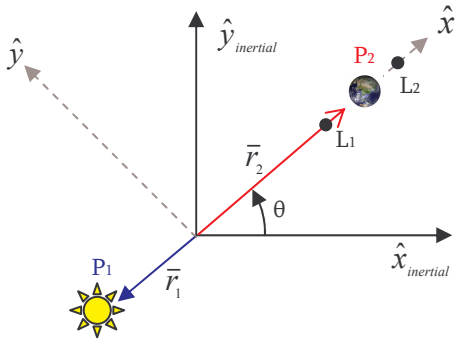

Figure 1: Circular Restricted Three-Body Problem.

Let $\bar{X} = [x \quad y \quad z \quad \dot{x} \quad \dot{y} \quad \dot{z}]^T$, then the general non-dimensional equations of motion of a spacecraft, relative to the system barycenter, are

$$\ddot{x} - 2\dot{y} - x = -\frac{(1-\mu)(x+\mu)}{r_1^3} - \frac{\mu(x-(x-\mu))}{r_2^3} \qquad [1]$$

$$\ddot{y} + 2\dot{x} - y = -\frac{(1-\mu)y}{r_1^3} - \frac{\mu y}{r_2^3} \qquad [2]$$

$$\ddot{z} = -\frac{(1-\mu)z}{r_1^3} - \frac{\mu z}{r_2^3} \qquad [3]$$

where

$$r_1 = \left((x+\mu)^2 + y^2 + z^2\right)^{1/2}$$
$$r_2 = \left((x-(1-\mu))^2 + y^2 + z^2\right)$$

The quantity μ is a non-dimensional mass parameter associated with the system. For the Sun-Earth/Moon system, $\mu \approx 3.0404 \times 10^{-6}$.

A more compact notation incorporates a pseudo-potential function, U, such that

$$U = \frac{(1-\mu)}{r_1} + \frac{\mu}{r_2} + \frac{1}{2}(x^2 + y^2) \qquad [4]$$

Then, the scalar equations of motion are rewritten in the form

$$\ddot{x} = U_x + 2\dot{y} = f_x(x, \dot{x}, y, \dot{y}, z, \dot{z}) \qquad [5]$$

$$\ddot{y} = U_y - 2\dot{x} = f_y(x, \dot{x}, y, \dot{y}, z, \dot{z}) \qquad [6]$$

$$\ddot{z} = U_z = f_z(x, \dot{x}, y, \dot{y}, z, \dot{z}) \qquad [7]$$

where the symbol U_j denotes the partial derivative of U with respect to j. Equations [1]-[3] or equations [5]-[7] comprise the dynamic model in the circular restricted three-body problem.

Given a solution to the nonlinear differential equations, linear variational equations of motion in the CR3BP can be derived in matrix form as

$$\dot{\delta\bar{X}}(t) = A(t)\,\delta\bar{X}(t) \qquad [8]$$

where $\delta\bar{X} = [\delta x \;\; \delta y \;\; \delta z \;\; \delta\dot{x} \;\; \delta\dot{y} \;\; \delta\dot{z}]^T$ represents variations with respect to a reference trajectory. Generally, the reference solution of interest is not constant. In this analysis, the reference trajectory is a Lissajous orbit, or a quasi-periodic orbit, near L2. This particular orbit was identified by NASA Goddard Space Flight Center (GSFC) as a possibly advantageous orbit for the TPF-O mission, and appears in Figure 2.

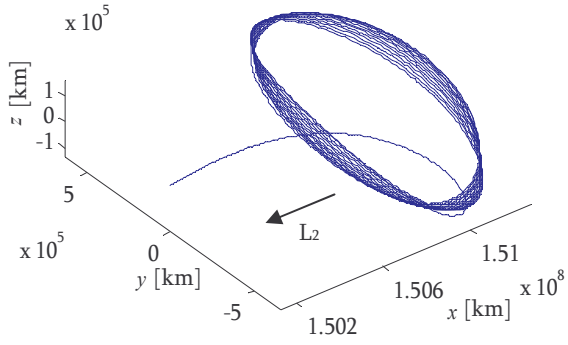

Figure 2: Nominal Lissajous Orbit for TPF-O Mission.

For the nominal Lissajous orbit, $A(t)$ is time-varying and of the form

$$A(t) = \begin{bmatrix} 0 & 0 & 0 & 1 & 0 & 0 \\ 0 & 0 & 0 & 0 & 1 & 0 \\ 0 & 0 & 0 & 0 & 0 & 1 \\ U_{xx} & U_{xy} & U_{xz} & 0 & 2 & 0 \\ U_{yx} & U_{yy} & U_{yz} & -2 & 0 & 0 \\ U_{zx} & U_{zy} & U_{zz} & 0 & 0 & 0 \end{bmatrix} \qquad [9]$$

The partials U_{kl} are also functions of time, although the functional dependence on time, t, has been dropped.

The general form of the solution to the system in equation [8] is

$$\delta\bar{X}(t) = \Phi(t, t_0)\,\delta\bar{X}(t_0) \qquad [10]$$

where $\Phi(t,t_0)$ is the state transition matrix (STM). The STM is a linear map from the initial state at the initial time, t_0, to a state at some later time, t, and thus offers an approximation for the impact of the variations in the initial state on the evolution of the trajectory. The STM must satisfy the matrix differential equation

$$\dot{\Phi}(t, t_0) = A(t)\,\Phi(t, t_0) \qquad [11]$$

given the initial condition,

$$\Phi(t, t_0) = I_{6x6} \qquad [12]$$

where I_{6x6} is the 6×6 identity matrix.

The STM at time t can be numerically determined by integrating equation [10] from the initial value. Since the STM is a 6×6 matrix, propagation of equation [10] requires the integration of 36 first-order, scalar differential equations. Because the elements of $A(t)$ depend on the reference trajectory, equation [10] must be integrated simultaneously with the nonlinear equations of motion to generate reference states. This requirement necessitates the integration of an additional 6 first-order equations, for a total of 42 differential equations.

DESCRIPTION OF CONTROL METHODS

Optimal nonlinear control and geometric control methods are compared to more traditional linear quadratic regulators and feedback linearization. The control strategies are implemented and evaluated for the TPF-O mission concept.

Time-Varying Linear Quadratic Regulator

Let the motion of a spacecraft moving in the CR3BP be described by

$$\ddot{x} = f_x\left(x, \dot{x}, y, \dot{y}, z, \dot{z}\right) + u_x \quad [13]$$

$$\ddot{y} = f_y\left(x, \dot{x}, y, \dot{y}, z, \dot{z}\right) + u_y \quad [14]$$

$$\ddot{z} = f_z\left(x, \dot{x}, y, \dot{y}, z, \dot{z}\right) + u_z \quad [15]$$

where f_x, f_y, and f_z are defined in equations [5]-[7] and $\bar{u}(t) = \begin{bmatrix} u_x & u_y & u_z \end{bmatrix}$ is an applied control (acceleration) vector. Let $\bar{X}^o(t)$ represent some reference motion that satisfies the system equations [13]-[15] and, then, $\bar{u}^o(t)$ denotes the control effort required to maintain $\bar{X}^o(t)$. Linearization about this reference solution yields a system of the form

$$\delta\dot{\bar{X}}(t) = A(t)\,\delta\bar{X} + B(t)\,\delta\bar{u}(t) \quad [16]$$

where $\delta\bar{X}(t)$ and $\delta\bar{u}(t)$ represent perturbations relative to $\bar{X}^o(t)$ and $\bar{u}^o(t)$, respectively. The matrix *A(t)* is defined in equation [9] and $B(t) = B = \begin{bmatrix} 0_{3x3} & I_{3x3} \end{bmatrix}^T$. The matrix *B(t)* is selected such that the control input can instantaneously change only the velocity of the satellite (not position).

To minimize some combination of the error state and required control, Bryson and Ho[29] employ a quadratic cost function

$$\min\ J = \frac{1}{2}\int_{t_0}^{t_f}\left(\delta\bar{X}(t)^T Q\,\delta\bar{X}(t) + \delta\bar{u}(t)^T R\,\delta\bar{u}(t)\right)dt \quad [17]$$

subject to the governing state equations in [16] with initial conditions $\delta\bar{X}(t_0) = \delta\bar{X}_0$. The matrices *Q* and *R* represent weighting factors on the state error and control effort, respectively. Both are positive definite. Because the individual state errors are decoupled from the required control, *Q* and *R* are diagonal matrices.

Application of the Euler-Lagrange theorem to the system in equations [16] and [17] yields the following optimality requirement on the control variable,

$$\delta\bar{u}(t) = -R^{-1}BP(t)\delta\bar{X}(t) \quad [18]$$

where *P(t)* is a solution of the matrix differential Riccati equation,

$$\dot{P}(t) = -A(t)^T P(t) - P(t)A(t) + P(t)BR^{-1}B^T P(t) - Q \quad [19]$$

subject to $P(t_f) = \begin{bmatrix} 0_{6x6} \end{bmatrix}$.

Equation [18] and [19] represent a two-point boundary value problem with 42 first-order, ordinary differential equations. However, for application to the CR3BP, this complexity can be avoided by exploiting the time invariance properties associated with the dynamical model. Marchand[28] develops a time transformation,

$$P(t_f - t) = G^{-1}S(t)G \quad [20]$$

where $G_{jj} = (-1)^{j-1}$, that enables simple forward integration to numerically solve a transformed Riccati matrix differential equation,

$$\dot{S}(t) = -A(t)^T S(t) - S(t)A(t) - S(t)BR^{-1}B^T S(t) + G^{-1}QG \quad [21]$$

Thus, the resulting optimal gain is defined as

$$K(t_f - t) = -R^{-1}B^T S(t)G \quad [22]$$

and can be implemented at each numerical time step. The nonlinear system of equations in [13]-[16] and the matrix differential equation in [21] are numerically integrated forward in time, subject to $\bar{X}(t_0) = \bar{X}^o(t_0)$ and $S(t_0) = 0$, respectively. Simultaneously, an optimal gain matrix is calculated at each integration time step and control is applied to the perturbed spacecraft motion.

It is notable that nearly the same optimal control gains can be computed by solving the algebraic Riccati equation at each integration step, rather than numerically integrating the differential Riccati equation. This method, although arguably less rigorous, requires far less computation time and, therefore, is very useful for preliminary analysis. Also, if the reference trajectory is periodic or well known a priori, the gain matrix can be computed and stored as a function of time for later implementation. If the integration time steps are defined such that no interpolation of *K(t)* is necessary, computation efficiency can be greatly improved.

Input State Feedback Linearization

One alternative to LQR control is input state feedback linearization (IFL). By implementing IFL, it is possible to specify desired characteristics of the state response.

To develop an IFL scheme, the motion of a spacecraft moving in the CR3BP is separated into linear and nonlinear components, such that

$$\ddot{x} = hx_{nonlinear} + hx_{linear} + u_x \quad [23]$$

$$\ddot{y} = hy_{nonlinear} + hy_{linear} + u_y \quad [24]$$

$$\ddot{z} = hz_{nonlinear} + hz_{linear} + u_z \quad [25]$$

where the h functions are defined as the linear and nonlinear terms in the equations [5]-[7], that is,

$$hx_{nonlinear} = -\frac{(1-\mu)(x+\mu)}{r_1^3} - \frac{\mu(x-(x-\mu))}{r_2^3} \quad [26]$$

$$hx_{linear} = 2\dot{y} + x \quad [27]$$

$$hy_{nonlinear} = -\frac{(1-\mu)y}{r_1^3} - \frac{\mu y}{r_2^3} \quad [28]$$

$$hy_{linear} = -2\dot{x} + y \quad [29]$$

$$hz_{nonlinear} = -\frac{(1-\mu)z}{r_1^3} - \frac{\mu z}{r_2^3} \quad [30]$$

$$hz_{linear} = 0 \quad [31]$$

There are many ways to implement feedback linearization. One option is to select the control, $\bar{u}(t)$, such that

$$\bar{u}(t) = \begin{bmatrix} u_x \\ u_y \\ u_z \end{bmatrix} = \begin{bmatrix} -hx_{nonlinear} \\ -hy_{nonlinear} \\ -hz_{nonlinear} \end{bmatrix} + \tilde{u}(t) \quad [32]$$

By first removing the nonlinear dynamics from the system, the control acceleration vector $\tilde{u}(t)$ is determined to produce the desired response characteristics of the linear, time-invariant dynamics. Linearization about a reference solution yields a subsystem of the form

$$\delta\dot{\bar{X}}(t)_{linear} = \tilde{A}\,\delta\bar{X}(t)_{linear} + B\,\delta\tilde{u}(t) \quad [33]$$

where B is defined above, and $\tilde{A}$ is determined from the linear dynamics of the spacecraft motion such that

$$\tilde{A} = \begin{bmatrix} 0 & 0 & 0 & 1 & 0 & 0 \\ 0 & 0 & 0 & 0 & 1 & 0 \\ 0 & 0 & 0 & 0 & 0 & 1 \\ 0 & 0 & 0 & 0 & 2 & 0 \\ 0 & 0 & 0 & -2 & 0 & 0 \\ 0 & 0 & 0 & 0 & 0 & 0 \end{bmatrix} \quad [34]$$

Because the pair $(\tilde{A}, B)$ is completely controllable, control effort is defined to place the poles of the linear system anywhere on the complex plane.

To minimize the state error with minimum control effort, $\delta\tilde{u}(t)$ is computed via LQR analysis. In this analysis, full-state feedback is assumed. The system is linear time-invariant, thus, the optimal control effort is defined by

$$\delta\tilde{u}(t) = -R^{-1}BP\delta\bar{X}(t)_{linear} \quad [35]$$

where the algebraic Riccati equation yields P,

$$-\tilde{A}^T P - P\tilde{A} + PBR^{-1}B^T P - Q = 0 \quad [36]$$

Feedback linearization offers both advantages and disadvantages over LQR control. This approach does not rely on a priori knowledge of the controller gain matrix since it is determined directly from the nonlinear system rather than the linear variational equations. It also allows a designer to specify desired response characteristics of the state. Thus, the stability of the system response can be more easily analyzed. However, in general, feedback linearization is implemented assuming full state feedback, which may or may not be available.

Impulsive Control via Differential Corrections

The use of a differential corrector is arguably the simplest method for computation of the required impulsive velocity change to reach a specified future position. An impulsive velocity change is also, potentially, the easiest to physically implement using available chemical thrusters. While LQR, IFL, and nonlinear methods may reveal advantageous trajectories that require less fuel, these approaches may be significantly more complicated to execute. It may be necessary to discretize and optimize the control results in order to use common propulsion systems.

Consider the general form of the discretized solution to the linear system in equation [8],

$$\delta\bar{X}_{k+1} = \Phi(t_{k+1}, t_k)\,\delta\bar{X}_k \quad [37]$$

where $\Phi(t_{k+1}, t_k)$ denotes the state transition matrix for the k^{th} segment associated with the nominal Lissajous orbit. The state can be partitioned into position and velocity components, $\delta\bar{r}$ and $\delta\bar{v}$, respectively, such that

$$\begin{bmatrix} \delta\bar{r}_{k+1} \\ \delta\bar{v}_{k+1}^- \end{bmatrix} = \Phi(t_{k+1}, t_k) \begin{bmatrix} \delta\bar{r}_k \\ \delta\bar{v}_k^+ \end{bmatrix} = \begin{bmatrix} \Phi_{rr} & \Phi_{rv} \\ \Phi_{vr} & \Phi_{vv} \end{bmatrix} \begin{bmatrix} \delta\bar{r}_k \\ \delta\bar{v}_k^- + \Delta\bar{V}_k \end{bmatrix} \quad [38]$$

where the superscript "+" or "-" signifies the beginning or end of a segment originating at time t_k, respectively, and $\Delta\overline{V}_k$ represents an impulsive maneuver applied at t_k. To accomplish the desired change in position, $\delta\overline{r}_{k+1}$, the required impulsive change in velocity (in the linear system) can be expressed as

$$\Delta\overline{V}_k = B_k^{-1}\left(\delta\overline{r}_{k+1} - \Phi_{rr}\delta\overline{r}_k\right) - \delta\overline{v}_k^- \quad [39]$$

Of course, in the nonlinear system, this linearly computed velocity change is inadequate. Differential corrections are incorporated in an iterative scheme to identify the precise maneuver that meets the end-state constraint to within the specified tolerance levels, as discussed in Howell and Barden.[30]

Nonlinear Optimal Control

To determine minimum fuel maneuvers for a spacecraft moving in the full nonlinear CR3BP, a traditional nonlinear optimal control problem is formulated. Let a cost function be defined as

$$\min J = \int_0^{t_f} \beta_x u_x^2 + \beta_y u_y^2 + \beta_z u_z^2 \, dt \quad [40]$$

where the vector $\overline{\beta} = \begin{bmatrix}\beta_x & \beta_y & \beta_z\end{bmatrix}$ is comprised of the weights on the corresponding control vector components, u_x, u_y, and u_z, defined in [32]. The Hamiltonian is then represented by

$$H = \beta_x u_x^2 + \beta_y u_y^2 + \beta_z u_z^2 + \lambda_1\dot{x} + \lambda_2\dot{y} + \lambda_3\dot{z} + \lambda_4\ddot{x} + \lambda_5\ddot{y} + \lambda_6\ddot{z} \quad [41]$$

where $\overline{\lambda}(t) = \begin{bmatrix}\lambda_1 & \lambda_2 & \lambda_3 & \lambda_4 & \lambda_5 & \lambda_6\end{bmatrix}$ is a vector of co-states and $\overline{\mathrm{X}}(t) = \begin{bmatrix}x & y & z & \dot{x} & \dot{y} & \dot{z}\end{bmatrix}$ is the vector of spacecraft states. The Euler equations are derived via the partial derivative of the Hamiltonian with respect to the state, as follows,

$$\dot{\lambda}_1 = -\frac{\partial H}{\partial x} = -\lambda_4\frac{\partial}{\partial x}(\ddot{x}) - \lambda_5\frac{\partial}{\partial x}(\ddot{y}) - \lambda_6\frac{\partial}{\partial x}(\ddot{z}) \quad [42]$$

$$\dot{\lambda}_2 = -\frac{\partial H}{\partial y} = -\lambda_4\frac{\partial}{\partial y}(\ddot{x}) - \lambda_5\frac{\partial}{\partial y}(\ddot{y}) - \lambda_6\frac{\partial}{\partial y}(\ddot{z}) \quad [43]$$

$$\dot{\lambda}_3 = -\frac{\partial H}{\partial z} = -\lambda_4\frac{\partial}{\partial z}(\ddot{x}) - \lambda_5\frac{\partial}{\partial z}(\ddot{y}) - \lambda_6\frac{\partial}{\partial z}(\ddot{z}) \quad [44]$$

$$\dot{\lambda}_4 = -\frac{\partial H}{\partial \dot{x}} = -\lambda_1 + 2\lambda_5 \quad [45]$$

$$\dot{\lambda}_5 = -\frac{\partial H}{\partial \dot{y}} = -\lambda_2 - 2\lambda_4 \quad [46]$$

$$\dot{\lambda}_6 = -\frac{\partial H}{\partial \dot{z}} = -\lambda_3 \quad [47]$$

Then, the conditions for optimality become,

$$\frac{\partial H}{\partial u_x} = 2u_x + \lambda_4 = 0 \quad [48]$$

$$\frac{\partial H}{\partial u_y} = 2u_y + \lambda_5 = 0 \quad [49]$$

$$\frac{\partial H}{\partial u_z} = 2u_z + \lambda_6 = 0 \quad [50]$$

This control strategy is implemented to maneuver a spacecraft from a specified initial state (both position and velocity) to a specified final position. Therefore, the boundary conditions include three "free" final conditions on both the state and co-state variables,

$$\overline{\mathrm{X}}(0) = \begin{bmatrix}x_0 & y_0 & z_0 & \dot{x}_0 & \dot{y}_0 & \dot{z}_0\end{bmatrix} \quad [51]$$

$$\overline{\mathrm{X}}(t_f) = \begin{bmatrix}x_f & y_f & z_f & free & free & free\end{bmatrix} \quad [52]$$

$$\overline{\lambda}(t_f) = \begin{bmatrix}free & free & free & 0 & 0 & 0\end{bmatrix} \quad [53]$$

The two-point boundary value problem is solved using a function (`bvp4c`) available in the Matlab Optimization Toolbox®. Final conditions for the "free" state and co-state elements are determined based upon knowledge of the optimal LQR solution for the same maneuver.

Geometric "Floquet" Control

Floquet control is an impulsive control strategy that exploits the phase space near a nominal orbit. At discrete intervals, a maneuver is performed in the direction of the center or stable manifolds. The main result of Floquet theory is that, for a time-varying periodic, linear system, the STM can be factored into two matrices, *E* and *J*, in the form

$$\Phi(t,0) = E(t)e^{Jt}E(0) \quad [54]$$

The matrix *J* is a constant matrix, usually in the Jordan normal form. Its diagonal entries, ω_i, are the Poincaré exponents, that is, the analog of the eigenvalues for constant-coefficient systems.

Because the nominal Lissajous orbit is not perfectly periodic, a similar halo orbit is successfully employed to approximate the surrounding phase space. The matrix *E(t)* corresponding to the halo orbit is periodic with period, *T*. Solving a Floquet problem for a periodic halo orbit over all time, thus, requires the determination of the constant matrix *J* and the periodic matrix *E(t)* over one period. Since the matrix

E is periodic, $E(0)=E(T)$ and, at $t=T$, equation [54] becomes

$$\Phi(T,0)=E(0)e^{JT}E(0) \qquad [55]$$

Thus, $E(0)$ is the matrix of eigenvectors of the monodromy matrix, $\Phi(t,t_0)$. The eigenvalues of the monodromy matrix, λ_i, are related to the Poincaré exponents ω_i, i.e.,

$$\lambda_i = e^{\omega_i T} \qquad [56]$$

After numerically integrating equation [11] over one period, the Poincaré exponents and the eigenvector matrix at $t=0$ are obtained. Since $E(t)$ is periodic and therefore bounded, the stability of the system is governed by ω_i (or λ_i) alone. Both the halo orbit and nominal Lissajous orbit of interest can be modeled as inherently unstable. In fact, the six-dimensional eigenstructure is characterized by one unstable eigenvalue (λ_1), one stable eigenvalue (λ_2), and four eigenvalues in the center subspace. Two of these neutrally stable eigenvalues are located on or near the unit circle (λ_3 and λ_4) and, given a perfectly periodic orbit, the remaining two are equal to one (λ_5 and λ_6). At any point in time, the perturbation $\delta\bar{X}(t)$ can be expressed in terms of any six-dimensional basis. The Floquet modes ($\bar{e}_j$), defined by the columns of $E(t)$, form a non-orthogonal six-dimensional basis. Hence,

$$\delta\bar{X}(t)=\sum_{j=1}^{6}\delta\bar{X}_j(t)=\sum_{j=1}^{6}c_j(t)\bar{e}_j(t) \qquad [57]$$

where $\delta\bar{X}_j(t)$ denotes the component of $\delta\bar{X}(t)$ along the j^{th} mode, $\bar{e}_j(t)$, and the coefficients $c_j(t)$ are determined as the elements of the vector $\bar{c}(t)$ defined by

$$\bar{c}(t)=E(t)^{-1}\delta\bar{X}(t) \qquad [58]$$

This Floquet structure is implemented by Gómez et al.[11] and, later, by Howell and Keeter[31] as the basis of a station keeping strategy for a single spacecraft evolving along a halo orbit. Both investigations determine the impulsive maneuver scheme that is required to remove the component of error in the direction of the unstable mode, $\delta\bar{X}_1(t)$ (as defined in [57]), at discrete intervals. Because impulsive maneuvers are calculated based on the phase space associated with a halo orbit, yet implemented on a spacecraft moving near a Lissajous orbit, additional error is incurred. This implies slightly larger impulsive maneuvers may be required to move a spacecraft state to the center subspace. However, in general, the error incurred is extremely small when compared to the magnitude of the required impulsive maneuver. Marchand and Howell, for instance, let

$$\delta\bar{X}_{desired}(t)=\sum_{j=2}^{6}\left(1+\alpha_j(t)\right)\delta\bar{X}_j(t) \qquad [59]$$

denote the desired perturbation relative to the reference orbit, where $\bar{\alpha}(t)$ is some, yet to be determined, coefficient vector. Note that the limits of the summation range from 2 through 6 which implies that the perturbation in the direction of the unstable mode, $\bar{e}_1$ has been removed. The linearized control problem then reduces to a computation of the impulsive maneuver, $\Delta\bar{v}(t)$, such that

$$\sum_{j=2}^{6}\left(1+\alpha_j(t)\right)\delta\bar{X}_j(t)=\sum_{k=1}^{6}\delta\bar{X}_k(t)+\begin{bmatrix}0_{3x1}\\ \Delta\bar{v}(t)_{3x1}\end{bmatrix} \qquad [60]$$

After some reduction, equation [60] can be rewritten in matrix form as

$$\begin{bmatrix}\delta\bar{X}_2(t) & \delta\bar{X}_3(t) & \delta\bar{X}_4(t) & \delta\bar{X}_5(t) & \delta\bar{X}_6(t) & \begin{matrix}0_{3x3}\\ I_{3x3}\end{matrix}\end{bmatrix} \times\begin{bmatrix}\bar{\alpha}(t)_{5x1}\\ \Delta\bar{v}(t)_{3x1}\end{bmatrix}=\delta\bar{X}_1(t) \qquad [61]$$

where $\bar{\alpha}$ represents a 5 x 1 vector formed by the α_j components in equation [59]. Therefore, the maneuver, $\Delta\bar{v}_{3x1}$, that is required to remove the unstable mode, $\bar{e}_1$, from the perturbation at any given time can be approximated from equations [61]. Howell and Keeter[31] identify this required $\Delta\bar{v}_{3x1}$ via a minimum norm solution. If the maneuver is constrained to the Sun-Earth line ($\hat{x}$ -direction), $\Delta\bar{v}_{1x1}$ is actually a scalar, and the system possesses an exact solution.

If exactly three modes are removed and control is possible in three directions, the system also possesses an exact solution. For example, Marchand and Howell[17] demonstrate the impulsive $\Delta\bar{v}_{3x1}$ that is required to remove the portion of the perturbation along the unstable and short period modes ($\bar{e}_1$, $\bar{e}_3$, and $\bar{e}_4$). It can be determined exactly from

$$\begin{bmatrix}\bar{\alpha}(t)_{3x1}\\ \Delta\bar{v}(t)_{3x1}\end{bmatrix}=\begin{bmatrix}\delta\bar{X}_2(t) & \delta\bar{X}_5(t) & \delta\bar{X}_6(t) & \begin{matrix}0_{3x3}\\ -I_{3x3}\end{matrix}\end{bmatrix}^{-1} \times\left(\delta\bar{X}_1(t)+\delta\bar{X}_3(t)+\delta\bar{X}_4(t)\right) \qquad [62]$$

Similarly, the $\Delta\bar{v}_{3x1}$ vector that is required to remove the unstable and long period modes ($\bar{e}_1$, $\bar{e}_5$, and $\bar{e}_6$) is exactly determined from

$$\begin{bmatrix} \bar{\alpha}(t)_{3x1} \\ \Delta\bar{v}(t)_{3x1} \end{bmatrix} = \begin{bmatrix} \delta\bar{X}_2(t) & \delta\bar{X}_3(t) & \delta\bar{X}_4(t) & 0_{3x3} \\ & & & -I_{3x3} \end{bmatrix}^{-1} \times \left(\delta\bar{X}_1(t) + \delta\bar{X}_5(t) + \delta\bar{X}_6(t)\right) \quad [63]$$

As formulated in equations [62] and [63], $\Delta\bar{v}_{3x1}$ is the impulsive control necessary to remove perturbations in the direction of one unstable mode and two semi-stable modes in the linearized system represented in equation [8] at a given time.

RESULTS FROM TPF-O MISSION ANALYSIS

TPF-O Mission Concept

The NASA Terrestrial Planet Finder-Occulter mission is an optical formation that will search for Earth-like planets in other solar systems. Two spacecraft are included in the formation: one telescope spacecraft and one occulter spacecraft. The telescope spacecraft moves near a nominal L_2 Lissajous orbit. During an observation period, the telescope and the occulter align along the direction to a star of interest in some inertial direction. The two spacecraft are required to maintain a fixed relative distance during this phase. During the transit, or maneuver, period there is no constraint on the geometry of the occulter and telescope. The "transit period" refers to the time period between t_1 and t_2, while the "observation period" denotes the time interval between t_2 and t_3, as illustrated in Figure 3.

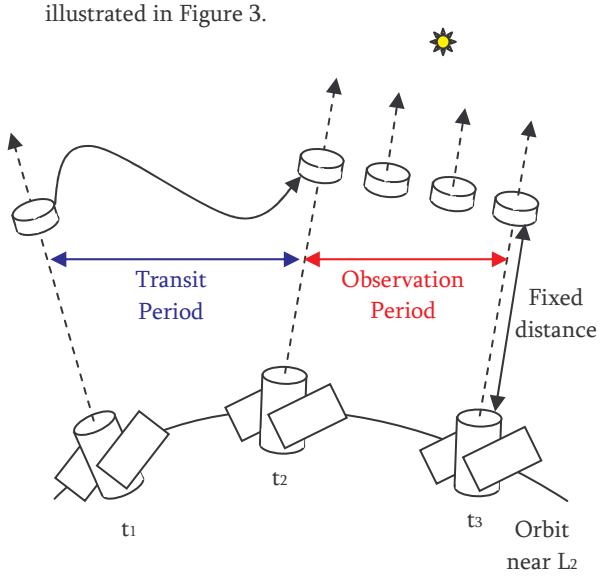

Figure 3: Schematic of TPF-O Mission Sequence.

The path of the occulter is dictated by a star sequence. This star sequence represents a list of stars that are in the same spectral class as the Sun, indicating a higher potential for the existence of nearby, orbiting Earth-like planets. The required observation time at each star and the specific length of time allotted for maneuvering between each observation is also included in the star sequence. In this analysis, two star sequences are used for comparison: Design Reference Mission (DRM) 4 and DRM 5. These sequences are specified as options for TPF-O. The general characteristics of the star sequences are compared in Table 1. Placement of the stars, in a given sequence on a celestial sphere, is noted in Figure 4.

Star Sequence	Mission Duration	Number of Observations	Distance to Occulter	Average Observation	Average Transit
DRM4	1832 days	134	72000 km	2.67 days	10.99 days
DRM5	1840 days	102	37800 km	3.24 days	14.80 days

Table 1: Features of DRM4 and DRM5 Sequences

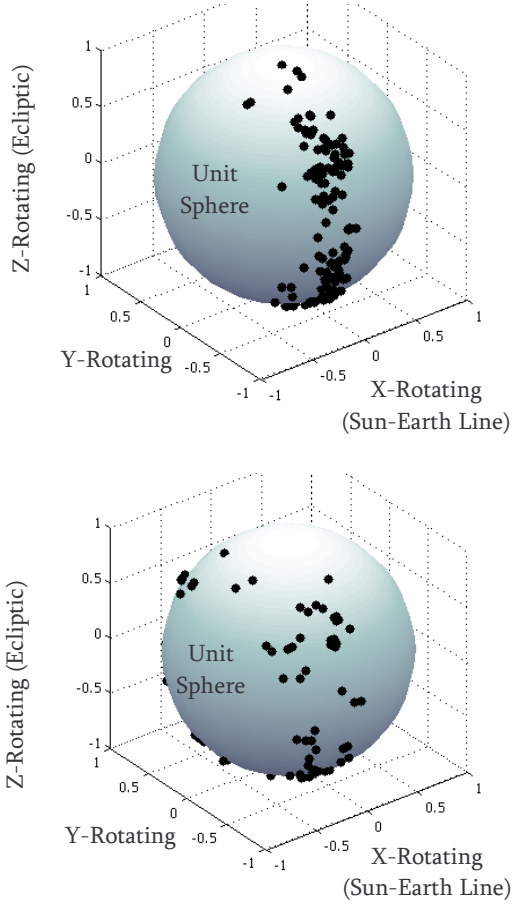

Figure 4: Star Sequences for DRM 4 (top) and DRM 5 (bottom).

Control Analysis Results

The various control strategies are implemented in differing combinations for DRM 4 and DRM 5. For example, in one scenario, a nonlinear optimal controller is used for transit between t_1 and t_2 (in Figure 3) and an LQR controller is used to track the star during an observation period. Alternatively, an impulsive maneuver can support the transit between t_1 and t_2, as well as t_2 and t_3; this approach implies that no star tracking occurred during the observation period. A summary of the different scenarios and the resulting required control effort is listed in Tables 2 and 3.

The first column in these tables, labeled "Total ΔV" is an estimate of the control effort required for the entire mission. Because each mission contains a different number of star targets, it may be helpful to determine the average control effort used for each star in the sequence. This appears in the second column labeled, "Ave. ΔV per star." In columns 3 and 4, the total control effort is divided into mission segments: transit and observation periods, respectively. Finally, the last column is a measure of only the control effort needed to track the star during the observation period. This number is defined as the amount of control necessary to maintain the occulter within a specified

Control Method	Total ΔV [km/s]	Ave. ΔV per star [m/s]	Transit ΔV [km/s]	Observation ΔV [km/s]	Star Track [m/s]
Impulsive Transit without Star Track	4.728	35.284	4.728	--	--
Impulsive Transit + Impulsive Star Track	5.783	43.157	2.795	2.947	--
Impulsive Transit + LQR Star Track	5.955	44.440	2.702	3.253	30.074
Impulsive Transit + IFL Star Track	5.966	44.522	2.704	3.263	30.166
LQR Transit + LQR Star Track	5.998	44.761	2.745	3.253	30.074
IFL Transit + IFL Star Track	6.067	45.275	2.804	3.263	30.166
NL Optimal Transit + Impulsive Star Track	5.802	43.299	2.855	2.947	--
NL Optimal Transit + LQR Star Track	6.103	45.545	2.850	3.253	30.074
NL Optimal Transit + IFL Star Track	6.111	45.604	2.848	3.263	30.166
Geometric Transit + Impulsive Star Track	6.792	50.687	3.845	2.947	--
Geometric Transit + LQR Star Track	6.804	50.776	3.551	3.253	30.074
Geometric Transit + IFL Star Track	6.811	50.828	3.548	3.263	30.166

Table 2: Required Control Effort for DRM 4.

Control Method	Total ΔV [km/s]	Ave. ΔV per star [m/s]	Transit ΔV [km/s]	Observation ΔV [km/s]	Star Track [m/s]
Impulsive Transit without Star Track	2.721	26.676	2.721	--	--
Impulsive Transit + Impulsive Star Track	2.899	28.422	1.506	1.392	--
Impulsive Transit + LQR Star Track	3.009	29.500	1.452	1.558	13.555
Impulsive Transit + IFL Star Track	3.013	29.539	1.451	1.561	13.581
LQR Transit + LQR Star Track	3.032	29.725	1.474	1.558	13.555
IFL Transit + IFL Star Track	3.111	30.500	1.549	1.561	13.581
NL Optimal Transit + Impulsive Star Track	2.995	29.363	1.603	1.392	--
NL Optimal Transit + LQR Star Track	3.101	30.402	1.543	1.558	13.555
NL Optimal Transit + IFL Star Track	3.104	30.431	1.543	1.561	13.581
Geometric Transit + Impulsive Star Track	3.213	31.500	1.821	1.392	--
Geometric Transit + LQR Star Track	3.298	32.333	1.740	1.558	13.555
Geometric Transit + IFL Star Track	3.302	32.373	1.741	1.561	13.581

Table 3: Required Control Effort for DRM 5.

tolerance of the desired state, after it has made a maneuver to reach that state.

A few observations are noted in the results from the control analysis. Tables 2 and 3 both indicate that the impulsive method, used during the transit period, requires the least amount of control effort. The geometric "Floquet" maneuvers require the most control effort during the transit period.

DRM 4 has a significantly higher average control effort per star than DRM 5, as indicated by column 2 of Tables 2 and 3. Upon further investigation, it was determined that this is a result of the larger distance between the telescope and the occulter: 72000km for DRM 4 as opposed to 38700km for DRM 5. As the occulter is placed further and further away from the nominal telescope orbit, the control cost tends to increase. This may be due, in part, to the longer distance traveled by the occulter to create the desired angle during each observation period.

The required control at each star can also be represented graphically, as plotted in Figures 5 and 6. Figure 5 illustrates a notional thrust profile for DRM 4. This profile corresponds to row 3 in Table 2: impulsive control during transit periods and LQR control during observation periods. The horizontal axis represents each star in the DRM 4 sequence. The vertical axis is the amount of control required at a particular star in the sequence. The red line represents the total required control effort for the DRM 4 mission. This control effort is divided into the control required for the observation period and that required for the transit period, that is, the green and the cyan line, respectively. The dark blue line corresponds to the amount of control required if the analysis is performed without CR3BP dynamics, in other words, if spacecraft is assumed to be moving in free space. It is notable that control effort required for spacecraft moving in free space is significantly higher than that required for spacecraft moving in the CR3BP. Thus, in this mission scenario, the natural

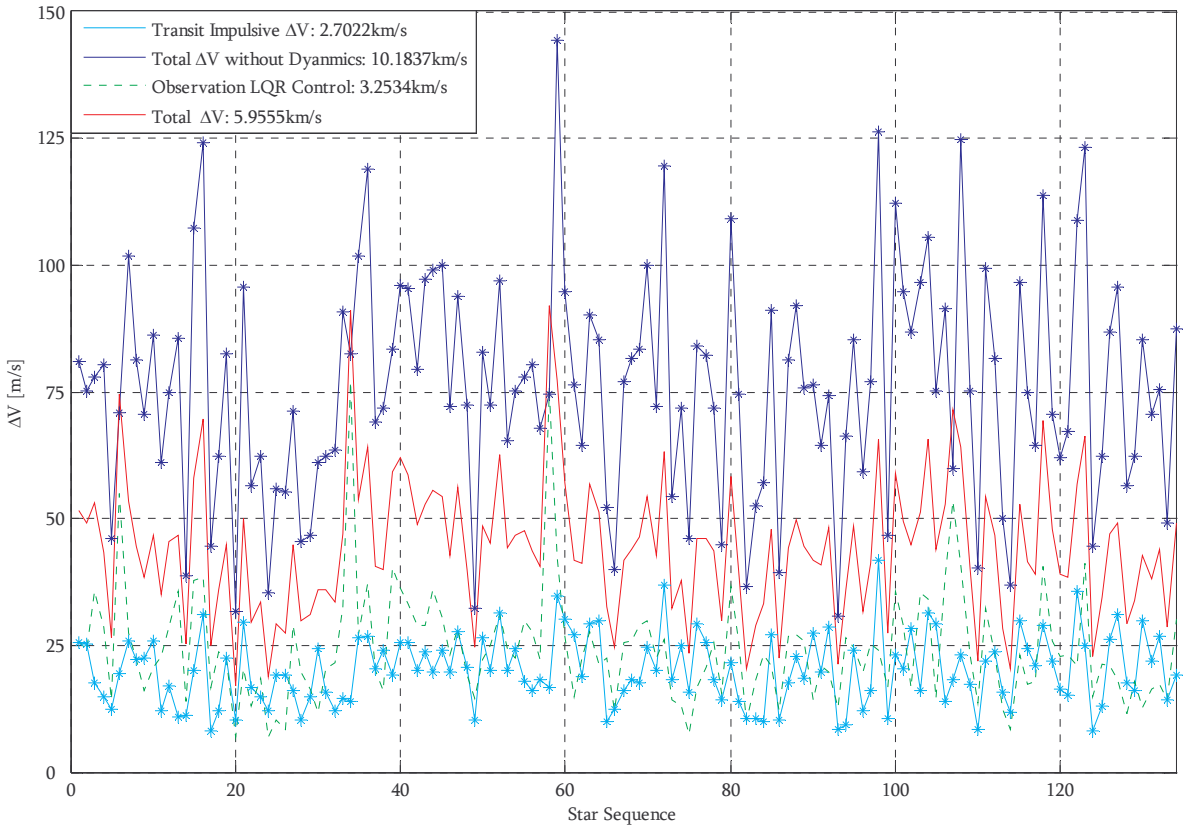

Figure 5: Notional Thrust Profile for DRM 4, Impulsive Control during Transit Periods and LQR Control during Observation Periods.

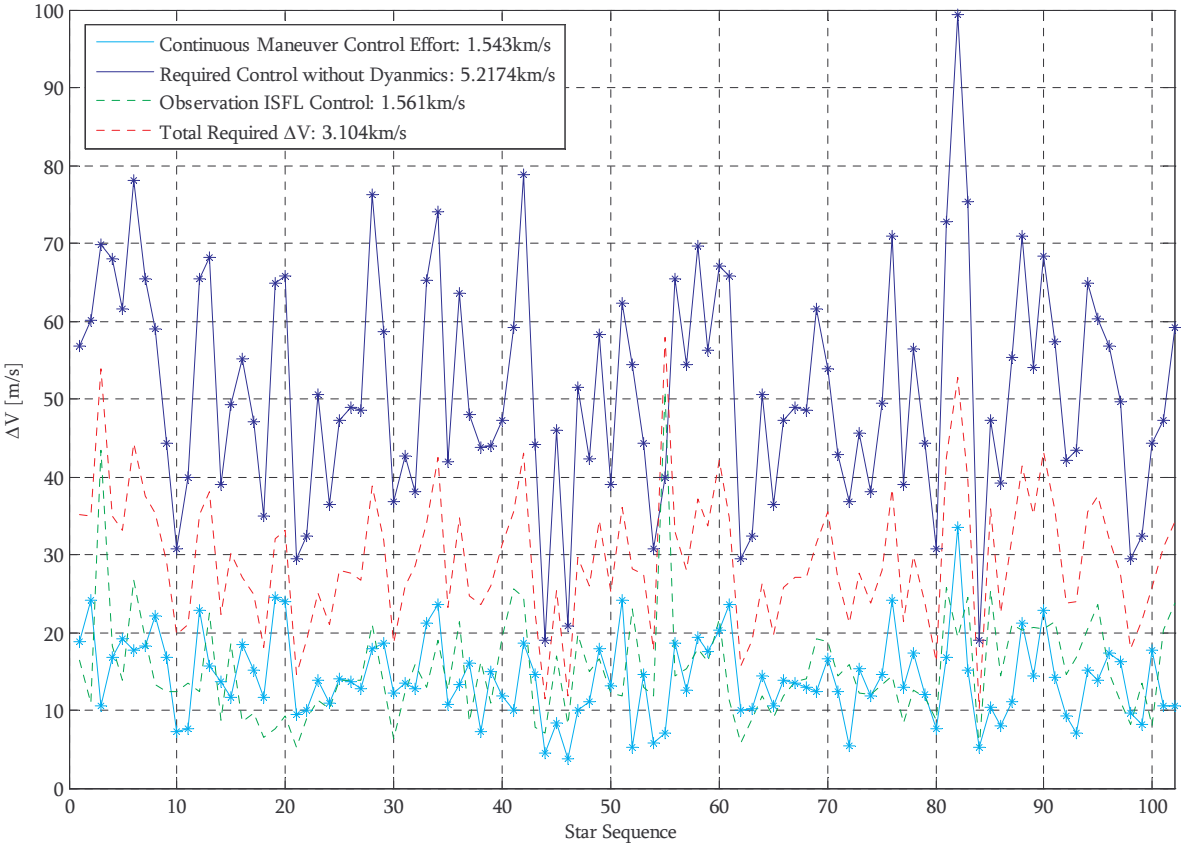

Figure 6: Notional Thrust Profile for DRM 5, Nonlinear Optimal Control during Transit Periods and Input-State Feedback Linearization Control during Observation Periods.

dynamics in this regime reduce the control cost of spacecraft maneuvers.

Similarly, Figure 6 illustrates a notional thrust profile for DRM 5. This profile corresponds to row 9 in Table 3: nonlinear optimal control during transit periods and input-state feedback linearization during observation periods. Again, the required control for a spacecraft formation moving in free-space is significantly higher than for a formation moving in the CR3BP.

LQR Control for TPF-O

For the TPF-O mission, the occulter position tolerances are provided in terms of a radial and transverse component. The radial direction is defined as the direction from the telescope to the target star, as illustrated in Figure 7. The transverse directions lay anywhere in a plane perpendicular to this radial direction. The occulter is constrained to remain within ±100km of the desired path in the radial direction and ±10m from the desired path in the transverse direction. Because the LQR problem is formulated in the CR3BP, it is difficult to determine the effect of the weighting matrices, Q and R, on the precision in the defined radial and transverse directions. Thus, the LQR problem is reformulated in terms of radial and transverse coordinates. Let the direction to the star target from the telescope be defined as $\hat{r} = r_1\hat{x} + r_2\hat{y} + r_3\hat{z}$ and the direction of the velocity of the telescope near the Lissajous orbit be defined as $\hat{v} = v_1\hat{x} + v_2\hat{y} + v_3\hat{z}$.

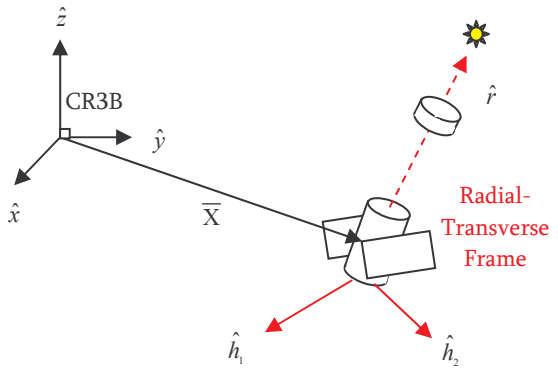

Figure 7: Coordinate Transformation from CR3BP to Radial-Transverse Frame.

Then, a vector perpendicular to both $\hat{r}$ and $\hat{v}$ is

$$\hat{h}_1 = \hat{r} \times \hat{v} \quad [64]$$

The direction $\hat{h}_1$ is defined as the first transverse direction. This choice is arbitrary, since the specific direction of the transverse coordinate frame does not effect the problem formulation. The new coordinate frame is completed by $\hat{h}_2$ such that,

$$\hat{h}_2 = \hat{r} \times \hat{h}_1 \quad [65]$$

To transform the original LQR problem into the new coordinate frame, a transformation matrix, C, is derived. This matrix transforms the perturbations $\delta\bar{X}$ to the new coordinate system $\delta\bar{Z}(t) = \begin{bmatrix} r & h_1 & h_2 & \dot{r} & \dot{h}_1 & \dot{h}_2 \end{bmatrix}$ such that

$$\delta\bar{X}(t) = C\delta\bar{Z}(t) \quad [67]$$

$$\delta\dot{\bar{X}}(t) = C\delta\dot{\bar{Z}}(t) + \dot{C}\delta\bar{Z}(t) \quad [68]$$

Substituting equations [67] and [68] into equation [16] yields,

$$\delta\dot{\bar{Z}}(t) = \left[C(t)^{-1} A(t) C(t) - C(t)^{-1}\dot{C}(t)\right]\delta\bar{Z}(t) + C(t)^{-1} B\bar{u}(t) \quad [69]$$

and, thus, the new cost function for the LQR formulation is

min

$$J = \frac{1}{2}\int_{t_0}^{t_f}\left(\delta\bar{Z}(t)^T Q_Z \delta\bar{Z}(t) + \delta\bar{u}(t)^T R_Z \delta\bar{u}(t)\right)dt \quad [70]$$

where the diagonal entries of Q_Z and R_Z now represent the weighting on the radial and transverse error components. In this analysis, the weighting matrices,

$$Q_Z = I_{6x6} \quad [71]$$

$$R_Z = diag\left(\begin{bmatrix} 10^{-5} & 10^{-10} & 10^{-10} \end{bmatrix}\right) \quad [72]$$

are sufficient in almost all cases to maintain the desired tolerances on the state. However, recall that only the relative magnitude of Q_Z and R_Z are important, not the exact numbers used.

Floquet Control for TPF-O

During a transit period, several small maneuvers maintain the spacecraft state near the center subspace of the reference Lissajous orbit. Because the Lissajous orbit is not perfectly periodic, a similar halo orbit is used to approximate the surrounding phase space while calculating the required velocity change.

Because the spacecraft should eventually reach a specified observation state (which may or may not be in the center subspace,) an impulsive targeting maneuver is required at some point during the transit period. This maneuver is added at the time when the smallest total amount of thrust is required to move to the desired observation location. A schematic of the geometric control method, as applied to the TPF-O mission, appears in Figure 8.

The blue line in the top plot in Figure 8 indicates the difference between the path of the spacecraft and the nominal Lissajous orbit in the rotating x-direction during one transit period (approximately 16 days). A small maneuver is applied at each blue star to keep

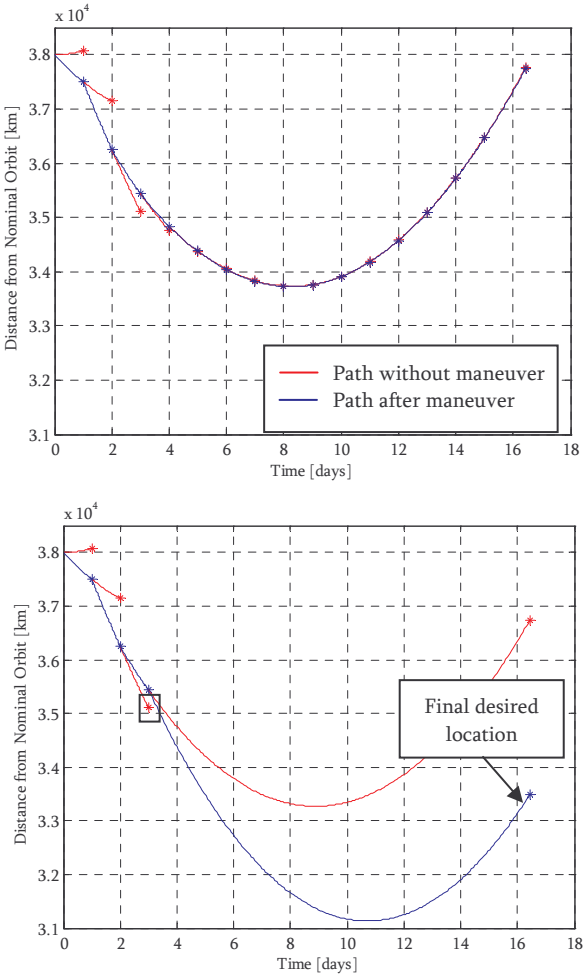

Figure 8: Geometric Control Method, Transit Period.

the spacecraft state near the center manifold during the transit period. Over longer periods of time, this trajectory is quasi-periodic. The red line in the top plot represents the spacecraft path if no maneuver is implemented. In the bottom plot, a point along the center manifold has been identified which minimizes the total required control effort to reach the specified observation point. This point appears in the black box. At this point, a targeting maneuver enables the vehicle to reach the final desired location. Again, the blue line indicates the trajectory of the spacecraft relative to the nominal orbit after the maneuvers have been performed. The red line indicates the path of the spacecraft without maneuvers.

Effectiveness of Control Methods on Mission Goals

During the transit period, no requirements exist on the position and velocity of the spacecraft formation to facilitate imaging. During the observation, though, the occulter must remain within 100km of the specified path in the radial direction and within 10m of the specified path in the transverse direction. When impulsive control is employed during the observation period, generally, these mission requirements are not met. However, when either input-state feedback linearization or LQR control are applied, weighting matrices can be selected such that position errors are within required tolerances.

An example of the required control effort and state error response in the transverse direction, during one observation period of the TPF-O mission, appears in Figure 9. The weighting matrices, Q_Z and R_Z, are defined such that the state error is just within the defined mission tolerances. In the first column of Figure 9, the required control in the transverse direction is plotted as a function of time for three different control methods. In the second column

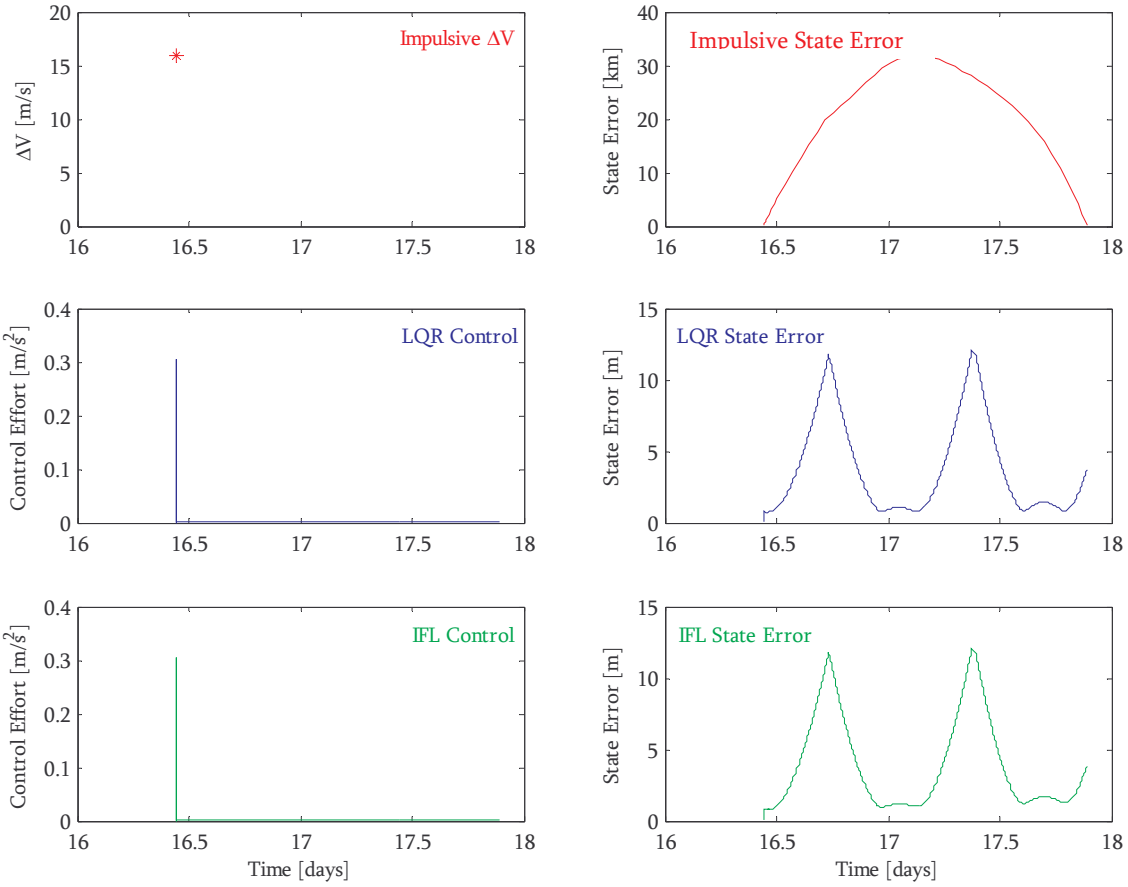

Figure 9: Required Control and State Error Response in the Transverse Direction over Observation Period: ± 10m.

of the plot, the state error in the transverse direction for the corresponding control method is displayed. This specific observation period corresponds to the first star of interest in the DRM 5 mission.

The typical required control effort and the state error response in the corresponding radial direction are represented in Figure 10. Because the position tolerance in the radial direction is relatively lenient, the state error response is higher in magnitude. This, again, results in part from the selection of Q_Z and R_Z. In the first column of the figure, the required control in the radial direction appears as a function of time for three different control methods applied to star tracking. The second column in the plot displays the state error in the radial direction for the corresponding control method.

Finally, an example of the path of both the occulter and telescope spacecraft can be seen in Figure 11. The trajectory of the telescope appears in blue, following the nominal Lissajous orbit. The occulter path is both red and cyan, indicating the transit and observation periods, respectively.

Concluding Remarks and Future Work

This work represents a preliminary comparison of various control strategies for the TPF-O mission concept. Error inclusion as well as estimation filters can be incorporated in future analyses. Also, the continuous control methods described may be discretized and optimized to provide competing control solutions for current chemical propulsion systems in a full ephemeris model.

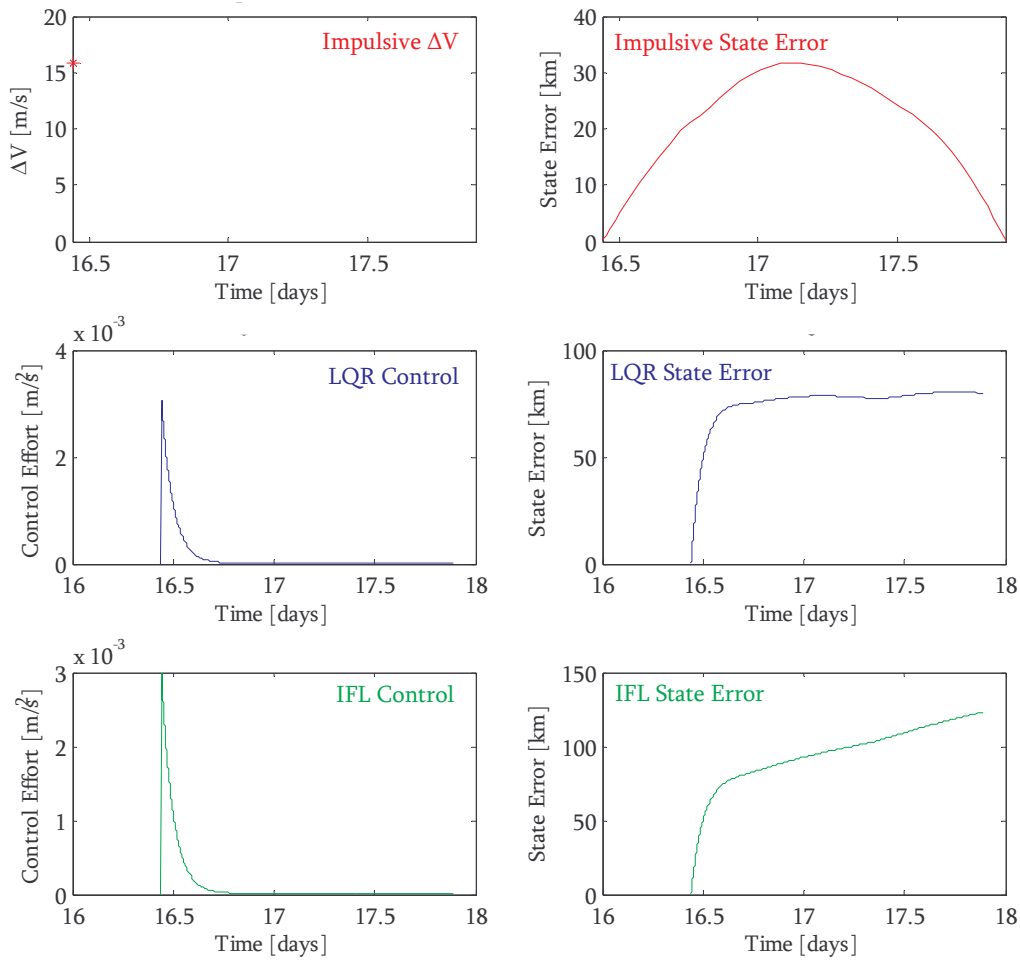

Figure 10: Required Control and State Error Response in the Radial Direction over Observation Period: ± 100km

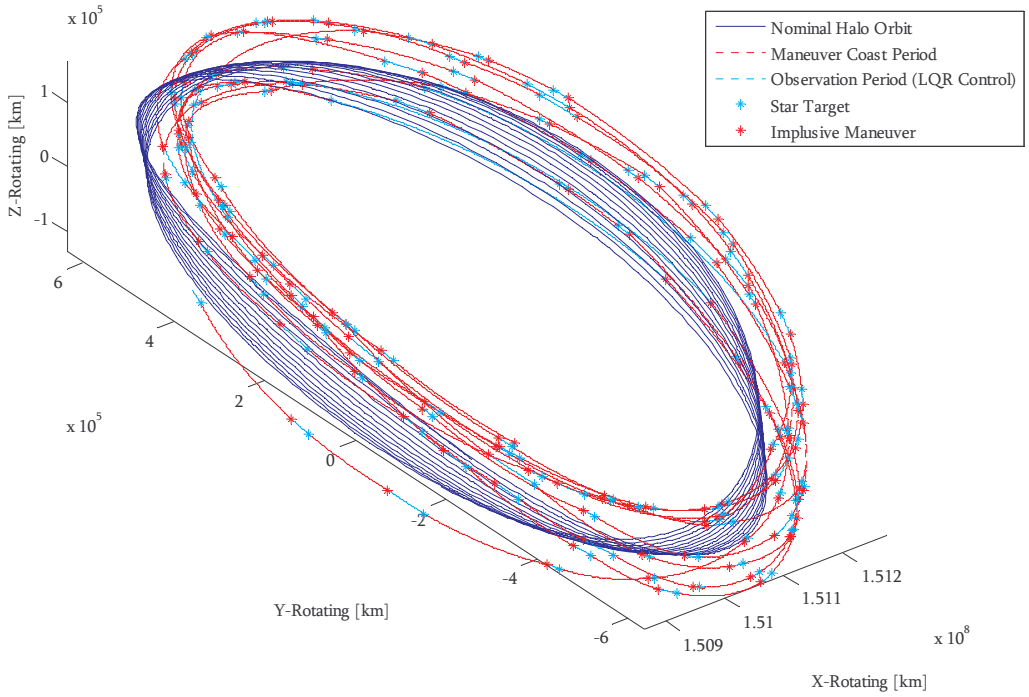

Figure 11: Occulter and Telescope Spacecraft Path, Impulsive Control during Transit and LQR Control during Observation Period.

For these two star sequences, it is observed that inclusion of the natural dynamics near the nominal Lissajous orbit in the model reduces the control cost for maneuvers. Such a result highlights the importance of including dynamics in mission control analyses in multi-body regimes.

Control costs can be reduced whenever it is possible to use a shorter baseline between the occulter and telescope spacecraft. The optimal relative distance between the occulter and telescope spacecraft, based on control cots, can be determined from further investigation.

Finally, and not surprisingly, the order and specific stars in a sequence affect the necessary control effort. However, the current mission design requirements specify stipulates a unique star sequence to be followed to maximize scientific results.

ACKNOWLEDGEMENTS

The authors would like to thank Dave Folta, Conrad Schiff, and the TPF-O working group at NASA Goddard Space Flight Center for providing information and guidance for the current study. This work was performed at Purdue University with support from NASA Goddard Space Flight Center under contract numbers NNG04GP69G and NNX06AC22G. Support was also provided from Purdue University via the Bilsland Dissertation Fellowship.

REFERENCES

1. Origins Science Subcommittee Members, "Origins Roadmap," National Aeronautics and Space Administration, © 2002.
2. Traub, W., S. Shaklan, and P. Lawson, "Prospects for Terrestrial Planet Finder (TPF-C, TPF-I, and TPF-O)," Proceedings of the Conference In the Spirit of Bernard Lyot: The Direct Detection of Planets and Circumstellar Disks in the 21st Century, University of California, Berkeley, California, June 4-8, 2007.
3. Cash, W., N. White, and M. Joy, "The Maxim Pathfinder Mission: X-Ray Imaging at 100 Micro-Arcseconds," Proceedings of the Soc. Photo-Opt. Instr. Eng., Vol. 4012, 2000, p. 258-269
4. Scharf, D. P., F. Y. Hadaegh, and S. R. Ploen, "A Survey of Spacecraft Formation Flying Guidance and Control (Part I): Guidance," American Control Conference, Denver, Colorado, June 4-6, 2003.
5. Scharf, D. P., F. Y. Hadaegh, and S. R. Ploen, "A Survey of Spacecraft Formation Flying Guidance and Control (Part II): Control," American Control Conference, Boston, Massachusetts, June 30-July 2, 2004.
6. Gurfil, P., and N. J. Kasdin, "Dynamics and Control of Spacecraft Formation Flying in Three-Body Trajectories," AIAA Guidance, Navigation, and Control Conference and Exhibit, Montreal, Canada, August 6-9, 2001.
7. Gurfil, P., M. Idan, and N. J. Kasdin, "Adaptive Neural Control of Deep-Space Formation Flying," American

Control Conference Proceedings, Anchorage, Alaska, Vol. 4, May 8-10, 2002, p. 2842-2847.
8. Luquette, R. J., and R. M. Sanner, "A Nonlinear Approach to Spacecraft Formation Control in the Vicinity of a Collinear Libration Point," AAS/AIAA Astrodynamics Conference Proceedings, Quebec, July 30-August 2, 2001, p. 437-445.
9. Hamilton, N. H., "Formation Flying Satellite Control Around the L2 Sun-Earth Libration Point," M.S. Thesis, George Washington University, Washington, DC, December 2001.
10. Folta, D., J. R. Carpenter, and C. Wagner, "Formation Flying with Decentralized Control in Libration Point Orbits," International Symposium: Spaceflight Dynamics, Biarritz, France, June 2000.
11. Gómez, G., K. C. Howell, J. Masdemont, and C. Simó, "Station-keeping Strategies for Translunar Libration Point Orbits," Advances in Astronautical Sciences, Vol. 99, Pt. 2, 1998, p. 949-967.
12. Gómez, G., M. Lo, J. Masdemont, and K. Museth, "Simulation of Formation Flight Near Lagrange Points for the TPF Mission," AAS/AIAA Astrodynamics Conference, Quebec, Canada, July 30-August 2, 2001.
13. Vadali, S. R., H. W. Bae, and K. T. Alfriend, "Design and Control of Libration Point Satellite Formations," 2004.
14. Li, H. M., and T. Williams, "Formation Keeping for Sun-Earth/Moon Libration Point Formation by Using Solar Radiation Pressure," AAS/AIAA 15th Space Flight Mechanics Meeting, Cooper Mountain, Colorado, January 23-27, 2005.
15. Howell, K. C., and B. G. Marchand, "Control Strategies for Formation Flight in the Vicinity of the Libration Points," AIAA/AAS Space Flight Mechanics Conference, Ponce, Puerto Rico, February 9-13, 2003.
16. Marchand, B. G., and K. C. Howell, "Formation Flight Near L1 and L2 in the Sun-Earth/Moon Ephemeris System Including Solar Radiation Pressure," AAS/AIAA Astrodynamics Specialist Conference, Big Sky, Montana, August 3-8, 2003.
17. Marchand, B. G. and K. C. Howell, "Spherical Formation Near the Libration Points in the Sun-Earth/Moon Ephemeris System," AAS/AIAA Spaceflight Mechanics Conference, Maui, Hawaii, February 8-11, 2004.
18. Carlson, B. A., H. J. Pernicka, and S. N. Balakrishnan, "Spacecraft Formation Flight about Libration Points," AIAA/AAS Astrodynamics Specialist Conference and Exhibit, Providence, Rhode Island, August 16-19, 2004.
19. Pernicka, H. J., B. A. Carlson, and S. N. Balakrishnan, "Spacecraft Formation Flight About Libration Points Using Impulsive Maneuvering," Journal of Guidance, Control, and Dyanmics, Vol. 29, No. 5, September-October 2006, p. 1122-1130.
20. Hyland, D. C., "Interferometric Imaging Concepts with Reduced Formation-Keeping Constraints," AIAA Space 2001 Conference, Albuquerque, New Mexico, August 2001.
21. Hussein, I. I., D. J. Scheeres, and D. C. Hyland, "Formation Path Planning for Optimal Fuel and Image Quality for a Class for Interferometric Imaging Missions," February, 2003.
22. Hussein, I. I., D. J. Scheeres, and D. C. Hyland, "Control of Satellite Formation for Imaging Applications," Proceedigns fo the American Control Conference, Copper Mountain, Colorado, January 23-27, 2005.
23. Hussein, I. I., D. J. Scheeres, and D. C. Hyland, "Optimal Formation Control for Imaging and Fuel Usage with Terminal Imaging Constraints," IEEE Conference on Control Applications, 2005.
24. Hussein, I. I., and A. M. Bloch, "Dynamic Coverage Optimal Control for Interferometric Imaging Spacecraft Formations," 43rd IEEE Conference on Decision and Control, Paradise Island, Bahamas, December 2004, p. 1812-1817.
25. Hussein, I. I., and A. M. Bloch, "Dynamic Coverage Optimal Control for Interferometric Imaging Spacecraft Formations (Part II): The Nonlinear Case," Proceedings fo the American Control Conference, 2005, p. 2391-2396.
26. Howell, K. C., and L. D. Millard, "Control of Satellite Imaging Formations in Multi-Body Regimes," IAF 57th International Astronautical Congress, Valencia, Spain, September 28-October 2, 2006.
27. Millard, L. D., and K. C. Howell, "Control of Interferometric Spacecraft Arrays for (u, v) Plane Coverage in Multi-Body Regimes," AAS/AIAA Spaceflight Mechanics Conference, Sedona, Arizona, January 28-February 1, 2007.
28. Marchand, B., "Spacecraft Formation Keeping Near the Libration Points of the Sun-Earth/Moon System," PhD Thesis, Purdue University, August, 2004.
29. Bryson, A. E., and Y. Ho, Applied Optimal Control: Optimization, Estimation, and Control, Hemisphere Publishing Corporation, New York, 1975.
30. Barden, B. T., and K. C. Howell, "Formation Flying in the Vicinity of Libration Point Orbits," *Advances in Astronautical Sciences*, Vol. 99, 1998, p. 969-988.
31. Howell, K.C., and T. M Keeter, "Station-Keeping Strategies for Libration Point Orbits: Target Point and Floquet Mode Approaches," AAS/AIAA Spaceflight Mechanics Meeting, Albuquerque, New Mexico, February 13-16, 1995.